CHINESE JOURNAL OF PHYSICS VOL. 49 , NO. 1 FEBRUARY 2011

Surface acoustic Bloch oscillations and multiple resonant Landau-Zener tunneling in a solid

Yu. A. Kosevich,[1,2,*] M. M. de Lima, Jr.,[2,†] P. V. Santos,[3] and A. Cantarero[2]

[1]*Semenov Institute of Chemical Physics, Russian Academy of Sciences, Moscow, Russia*
[2]*Materials Science Institute, University of Valencia, Valencia, Spain*
[3]*Paul-Drude-Institut fuer Festkoerperelektronik, Berlin,Germany*

(Received April 12, 2010)

We present a theoretical description and results of the first experimental observation of Bloch oscillations, Wannier–Stark ladders, and resonant Landau–Zener tunneling of surface acoustic waves in perturbed grating structures made of gold stripes on a $LiNbO_3$ substrate. Our model provides a quantitative description of all the relevant features of the experimental observations, including multiple resonant Landau–Zener transitions between anticrossed surface acoustic Wannier–Stark states, which originate from neighboring acoustic minibands.

PACS numbers: 62.65.+k, 63.22.-m, 43.35.+d

I. INTRODUCTION

Bloch oscillations (BOs) and Landau–Zener tunneling (LZT) are the fundamental phenomena associated with the quantum dynamics of a particle in a periodic potential subjected to an external static force. BOs of the wave packet group velocity result from the interplay between the particle-like acceleration caused by a constant driving force and the wave-like Bragg reflection in the periodic potential. These BOs lead to the formation of a Wannier–Stark ladder (WSL) of localized states in a perturbed periodic potential. LZT to higher-energy bands is responsible for anticrossing between the WSLs originating from neighboring bands, which in turn causes spatial delocalization of the WS states. BOs and LZT of electrons have been impressively demonstrated after the advent of semiconductor superlattices [1, 2]. Subsequently, these investigations have been extended to various physical systems such as cold atoms and Bose–Einstein condensates in accelerating optical lattices [3, 4] and optical waves in photonic lattices [5, 6].

In general, Bragg reflections can cause BOs of waves of any nature (electronic, optical, acoustic, or matter waves) in a lattice with a weak linear gradient of the lattice potential, e.g., [7, 8]. Recently, considerable efforts have been made by researchers in the field of phononics to observe BOs, WSLs, and LZT [9]. For instance, BOs and WSL states have been predicted for semiconductor multilayer solid structures based on acoustic-phonon cavities [10]. Vibration WSLs have been observed in one-dimensional (1D) elastic chains [11]. The existence of acoustic BOs, WSLs, and LZT has been demonstrated in the ultrasonic superlattice made of layers of a solid polymer, with 1D water cavities between the layers [12]. The existence of acoustic BOs, WSLs, and LZT has also been demonstrated in 2D

phononic crystals made of rigid cylinders in water [13, 14]. However, such phenomena have not been observed in solid-state devices based on phononic structures fabricated by standard lithography techniques.

We demonstrated that the fundamental phenomena related to quantum wave transport in a perturbed periodic potential, such as BOs, WSLs, and LZT, can be studied by using surface acoustic waves (SAWs) in a solid (see also Ref. [15]). We developed a theoretical model for providing a quantitative description of our experimental observations, including *multiple* Landau–Zener-like transitions between anticrossed surface acoustic Wannier–Stark states. As opposed to previous studies in which bulk superlattices were used for carrying out observations, the present study involves the use of planar geometry for the realization of surface acoustic BOs, WSLs, and LZT, and hence enables direct measurement of the elastic field distribution of the corresponding Wannier–Stark and Landau–Zener eigenstates.

II. THEORY

In our approach, we employ SAW cavities separated by acoustic Bragg reflectors (BRs). BRs are efficient barriers and show high reflectivity for an incoming wave-packet, despite the fact that the reflection amplitude (r) of a single thin stripe is usually very small: $r \sim h/\lambda$ for $h \ll \lambda$, where h is the thickness of the stripe and λ is the SAW wavelength. The appropriate number of stripes N_s in a BR can be determined from the condition $rN_s \sim 1$. By performing transfer-matrix (TM) calculations, we model SAW propagation in grating structures as the propagation of a scalar acoustic wave through the 1D multilayer system, which consists of two distinct types of layers having the same effective shear modulus but different effective densities. The difference between the effective densities of the two layers causes a difference in the acoustic wave velocities in the corresponding layers. This velocity difference in turn causes a difference ΔV_R in the velocities of the Rayleigh SAWs at a free surface and a surface perturbed by mass loading [16]: $\Delta V_R/V_R \sim -4h/\lambda$, as has been observed in the case of a gold-stripe grating on a $LiNbO_3$ substrate [17]. The scalar displacement in this model is proportional to the vertical and in-plane elastic displacements of the Rayleigh SAWs, e.g., Ref. [18]. This nonperturbative model, which is valid for gratings made of a material with relatively high mass density and low transverse acoustic velocity when $h \ll \lambda$, accounts for and quantitatively describes the main features of SAW transport in the perturbed periodic potentials considered.

III. EXPERIMENT

The unperturbed grating structure used in our experiment consists of six BRs separated by five identical free-surface $LiNbO_3$ $3\lambda/2$ cavities (see [15] for details of the setup). Each BR consists of 20 $\lambda/4$ gold stripes (corresponding to a width of ~ 2.8 μm) separated by a $\lambda/4$ free-surface $LiNbO_3$ spacing. In order to emulate the driving force for SAWs, structures with perturbed cavities are produced. Namely, the lengths of the cavities are

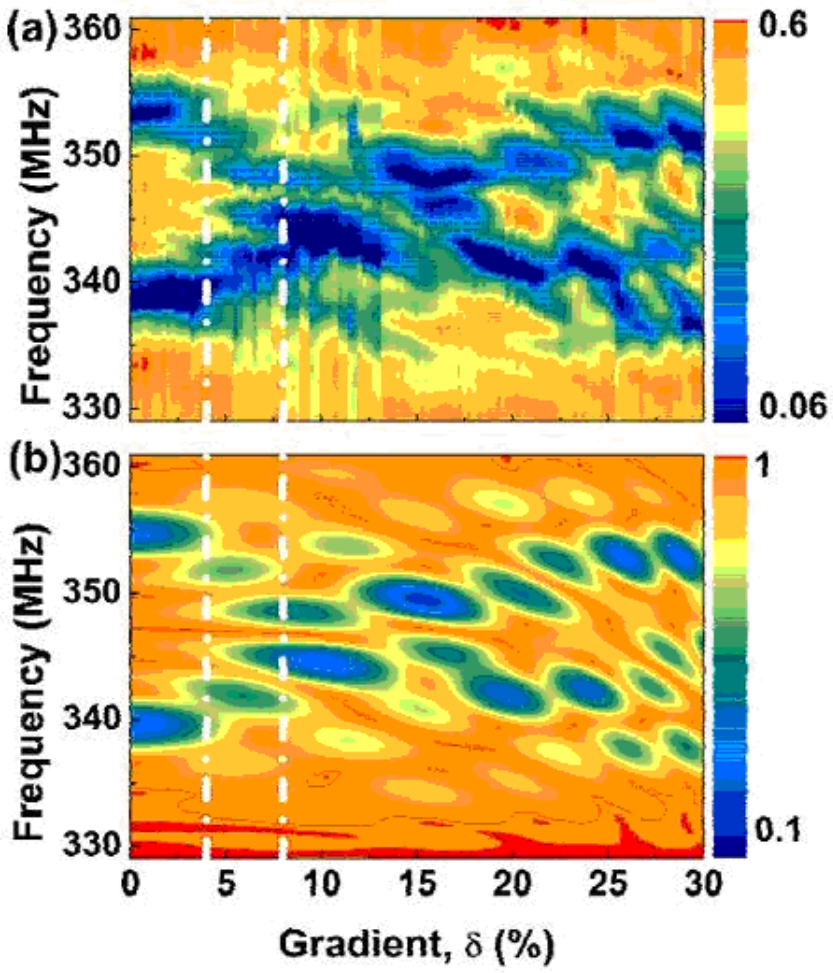

FIG. 1: Logarithmic-scale plot of measured (a) and calculated (b) spectra for surface acoustic wave transmission through weakly coupled cavity structures for various design gradients δ. Total thickness of composite gold stripes with 10 nm NiCr adhesion layers is 60 nm in the experiment, and that for pure gold stripes is 50 nm in the simulations. Vertical dashed-dotted lines indicate the region corresponding to the Wannier–Stark ladder states.

changed according to the constant gradient δ in the resonant frequency of the uncoupled cavities.

The experimental results obtained for SAW propagation through 60-nm-thick grating structures whose design gradient is in the range $0 \leq \delta \leq 30\%$ are shown in Fig. 1(a). The plot presents the transmission amplitude through the structure on a logarithmic scale. The vertical and horizontal axes show the SAW frequency and δ, respectively. The grid on the horizontal scale has steps of $\delta = 0.25\%$, and each step corresponds to a different device consisting of a grating structure inserted between a pair of interdigital transducers. The SAW transmission is measured by means of a network analyzer, which is normalized by a refer-

ence signal obtained from a delay line without any grating. The vertical dashed lines divide the plot into three regions. In the region $\delta \leq 4\%$, the gradient is small and the transmission in the band gap is governed by miniband wave transport, where the Fabry–Perot peaks are associated with the coupled cavities. The wave functions within this frequency range are extended throughout the structure. For the $4\% \leq \delta \leq 8\%$region, the resonant frequencies show a linear dependence on the design gradient, as is typically observed for WSLs; in this region, the coupling between the cavities is suppressed and the wave functions associated with the ladder states are localized mainly at individual cavities. The phenomena observed in the $\delta > 8\%$ region are highly complex because several states originating from the higher and lower transmission bands undergo anticrossing with the WSL states generated by the cavities. These anticrossings correspond to the brighter regions in the Fig. 1(a) since the corresponding transmission amplitudes are high owing to resonant LZT. Apart from the ordinary anticrossings between two WSL states, *multiple* Landau–Zener transitions are observed in these graphs: a few triple anticrossings (for $\delta \approx 16\%$) and one quadruple LZT (for $\delta \approx 25\%$).

Figure 1(b) shows the results of the TM calculations carried out for pure gold stripes with a thickness of 50 nm. There is excellent qualitative and quantitative agreement between the experimental and calculation results. All the relevant features of the experimental plot, including the positions of the main single and multiple anticrossings, can be clearly assigned to the corresponding features determined from the calculations. It is worth mentioning that we use only two parameters in our TM calculations. One is the gold-stripe thickness h, which defines the width and depth of the band gap produced by the BRs, as well as the value of the center frequency of the unperturbed miniband f_C. The best fit of the experimental data is obtained when h is assumed to be 50 nm in the calculations, whereas the actual thickness of the metal grating is approximately 60 nm. The other parameter used in our calculations is the SAW velocity in the unperturbed $LiNbO_3$ layer. The velocity of SAWs v_{SAW} in metal grating structures is between the velocities of SAWs in completely metallized surfaces and free surfaces [19]. The v_{SAW} value used in the present calculation (3920 m/s) is between the experimentally determined free-surface velocity v_0 (3983 m/s) and the velocity at a completely metallized surface v_{MET} (3880 m/s), as determined for $LiNbO_3$ in the propagation direction [19]. This v_{SAW} is chosen by fine-tuning the calculated f_C so that it becomes close to the experimental f_C. Thus, the aforementioned v_{SAW} value is obtained by taking into account the piezoelectric effect and partial surface metallization, in addition to the surface mass loading effect caused by the metal grating.

In order to confirm the presence of surface acoustic BOs for the frequency region in which the WSL is observed, we used the time-domain configuration of the network analyzer and measured the amplitude of the Fourier-transformed transmission signal for samples with different δ values. The observed dependence of the frequency of surface acoustic BOs on δ is in good agreement with the TM modeling results (see [15]). Our model also gives a quantitative explanation of the observed effective *acoustic field screening* in the designed perturbed SAW cavities, which are separated by unperturbed acoustic BRs. Namely, the dimensionless gradient of the resonant frequency of the coupled cavities δ_f is proportional to δ but is substantially different from δ. This difference between δ_f and δ is due to the fact

that in our design, the BRs remain unperturbed, and hence, the driving force is present only in the cavities. Thus, the average driving force acting on the SAW wave packet propagating through the structure is reduced owing to the effective acoustic field screening. From the TM calculations, we obtain $\delta = 7.3\delta_f$ and $\delta = 7.1\delta_f$ for the 120- and 60-nm-thick samples, respectively. The obtained δ/δ_f ratios are very close to the structural ratio (7.5), i.e., the ratio of the spatial period $d = 45\lambda/4$ and the length of the unperturbed cavities $L_0 = 3\lambda/2$.

Distribution along the surface of the vertical component of the elastic displacements has been measured directly by means of Michelson interferometry [20]. Both surface acoustic Wannier–Stark eigenstates and Landau–Zener eigenstates have been studied (see [15]).

IV. DISCUSSION

We demonstrate that the fundamental effects of wave transport in a perturbed periodic potential, such as acoustic BOs, WSLs, and LZT, can be studied by using surface acoustic waves on a solid substrate. We used perturbed surface gratings of gold stripes on a $LiNbO_3$substrate to observe these time- and frequency-domain dynamical surface phenomena. Our numerical simulations provide a quantitative description of the relevant features of our experimental observations, including multiple Landau–Zener transitions between the anticrossed surface acoustic Wannier–Stark states, which originate from different acoustic minibands. The planar geometry used for the realization of surface acoustic BOs and LZTs enables direct measurement of the elastic field distribution of the corresponding Wannier–Stark and Landau–Zener eigenstates.

V. CONCLUSIONS

Our observations demonstrate that surface acoustic waves on a solid substrate can be used for the detection and visualization of the surface acoustic analogs of fundamental quantum-mechanical phenomena. In addition, the grating structures used in this study allow us to observe and manipulate the effective acoustic field screening effect and determine the acoustic analog of the dielectric constant, knowledge of which is important for a comprehensive interpretation of the surface acoustic analogs of fundamental quantum-mechanical phenomena.

Acknowledgments

We thank W. Seidel for assistance in device fabrication. Yu. A. K. is grateful to Materials Science Institute of the University of Valencia for its hospitality and support and to the financial support extended by RFBR (grant No. 08-02-00368). We also thank Spanish Ministry of Science and Innovation for their financial support (grant No. TEC2009-12075).

References

* Electronic address: yukosevich@gmail.com
† Electronic address: mmlimajr@uv.es

[1] J. Feldmann *et al.*, Phys. Rev. B **46**, 7252 (1992).
[2] H. Schneider *et al.*, Phys. Rev. Lett. **65**, 2720 (1990).
[3] M. Ben Dahan *et al.*, Phys. Rev. Lett. **76**, 4508 (1996).
[4] C. F. Bharucha *et al.*, Phys. Rev. A **55**, 857 (1997).
[5] T. Pertsch *et al.*, Phys. Rev. Lett. **83**, 4752 (1999).
[6] M. Ghulinyan *et al.*, Phys. Rev. Lett. **94**, 127401 (2005).
[7] Yu. A. Kosevich, Phys. Rev. B **63**, 205313 (2001).
[8] A. Modinos *et al.*, Physica B **296**, 167 (2001).
[9] M. Sigalas *et al.*, Z. Kristallogr. **220**, 765 (2005).
[10] N. D. Lanzillotti-Kimura, A. Fainstein, and B. Jusserand, Phys. Rev. B **71**, R041305 (2005).
[11] L. Gutierrez *et al.*, Phys. Rev. Lett. **97**, 114301 (2006).
[12] H. Sanchis-Alepuz, Yu. A. Kosevich, and J. Sánchez-Dehesa, Phys. Rev. Lett. **98**, 134301 (2007).
[13] J. Sánchez-Dehesa, H. Sanchis-Alepuz, Yu. A. Kosevich, and D. Torrent, J. Acoust. Soc. Am. **120**, 3284 (2006).
[14] Z. He *et al.*, Phys. Rev. E **76**, 056605 (2007).
[15] M. M. de Lima, Jr., Yu. A. Kosevich, P. V. Santos, and A. Cantarero, Phys. Rev. Lett. **104**, 165502 (2010).
[16] Yu. A. Kosevich, E. S. Syrkin, and A. M. Kossevich, Progr. Surf. Sci. **55**, 59 (1997).
[17] D. H. Hurley and K. L. Telschow, Phys. Rev. B **66**, 153301 (2002).
[18] J. K. Knowles, J. Geophys. Res. **71**, 5480 (1966).
[19] G. Feuillard *et al.*, J. Appl. Phys. **74**, 6523 (1993).
[20] M. M. de Lima, Jr., and P. V. Santos, Rep. Prog. Phys. **68**, 1639 (2005).